

## Application of a gateless AlGaIn/GaN HEMT sensor for diesel soot particulate detection

Sokolovskij, Robert; Zheng, Hongze; Li, Wenmao; Zhou, Guangnan ; Wang, Qing; Zhang, Guoqi; Yu, Hongyu

**DOI**

[10.1016/j.snb.2021.130811](https://doi.org/10.1016/j.snb.2021.130811)

**Publication date**

2021

**Document Version**

Final published version

**Published in**

Sensors and Actuators B: Chemical

**Citation (APA)**

Sokolovskij, R., Zheng, H., Li, W., Zhou, G., Wang, Q., Zhang, G., & Yu, H. (2021). Application of a gateless AlGaIn/GaN HEMT sensor for diesel soot particulate detection. *Sensors and Actuators B: Chemical*, 349, 1-8. Article 130811. <https://doi.org/10.1016/j.snb.2021.130811>

**Important note**

To cite this publication, please use the final published version (if applicable).  
Please check the document version above.

**Copyright**

Other than for strictly personal use, it is not permitted to download, forward or distribute the text or part of it, without the consent of the author(s) and/or copyright holder(s), unless the work is under an open content license such as Creative Commons.

**Takedown policy**

Please contact us and provide details if you believe this document breaches copyrights.  
We will remove access to the work immediately and investigate your claim.



## Application of a gateless AlGaIn/GaN HEMT sensor for diesel soot particulate detection

Robert Sokolovskij<sup>a,b,c,d</sup>, Hongze Zheng<sup>a,b,c,d</sup>, Wenmao Li<sup>a,b,c,d</sup>, Guangnan Zhou<sup>a,b,c,d,e</sup>, Qing Wang<sup>a,b,c,d</sup>, Guoqi Zhang<sup>f</sup>, Hongyu Yu<sup>a,b,c,d,\*</sup>

<sup>a</sup> School of Microelectronics, Southern University of Science and Technology, Shenzhen 518055 China

<sup>b</sup> Engineering Research Center of Integrated Circuits for Next-Generation Communications, Ministry of Education, Southern University of Science and Technology, Shenzhen 518055, China

<sup>c</sup> GaN Device Engineering Technology Research Center of Guangdong, Southern University of Science and Technology, Shenzhen, 518055, China

<sup>d</sup> The Key Laboratory of the Third Generation Semi-conductor, Southern University of Science and Technology, Shenzhen 518055, China

<sup>e</sup> Department of Materials Engineering, The University of British Columbia (UBC), Vancouver, British Columbia, V6T 1Z4 Canada

<sup>f</sup> Department of Microelectronics, Delft University of Technology, 2628 CD Delft, the Netherlands

### ARTICLE INFO

#### Key words:

AlGaIn/GaN  
HEMT  
2DEG  
Soot sensor  
On-board diagnostics  
Diesel soot

### ABSTRACT

A particulate matter micro-sensor for automotive exhaust systems based on a gateless wide-bandgap AlGaIn/GaN high electron mobility transistor was developed and tested. Soot particles were generated by a laminar diesel flame and characterized with Raman spectroscopy, thermogravimetric analysis and scanning electron microscopy. Particle adsorption at the rate of 0.25 µg/min on the sensor surface resulted in 5.52% sensing response after 20 s and large signal variation of 4.44 mA, indicating fast response time. Saturated response of 34.72% (27.94 mA) was obtained after 10 min of deposition. The sensitivity towards soot is attributed to the modulation of the two-dimensional electron gas density by charged particles on the sensing surface. After soot deposition, the sensor was successfully regenerated by thermal oxidation of the carbonaceous particles at 600 °C. The sensing response remained unchanged post-regeneration indicating high temperature stability and harsh environment operation compatibility of the demonstrated GaN-based sensor. Nevertheless, interconnect metal optimization is still required to mitigate high-temperature interdiffusion.

### 1. Introduction

Incomplete combustion of hydrocarbon fuels produces solid carbonaceous particulates referred to as soot [1], which significantly contribute to air pollution in densely populated areas. Exposure to particulate matter (PM) has been linked to cardio-respiratory diseases, cancer, and premature death [2]. Major sources of these particles are diesel powered internal combustion engines, that are widely used by various industries due to their high efficiency and reliability combined with lower fuel consumption [3]. Automotive manufacturers are required to fit diesel particulate filters (DPF) in exhaust systems to comply with government regulations [4]. An on-board diagnostics (OBD) system with a soot detector is also required to continuously monitor the efficiency of soot collection, detect possible failures, and regenerate the DPF [5].

Until recently, soot loading and regeneration frequency of the DPF

were estimated by monitoring the exhaust gas pressure drop across the filter. This method is no longer sufficient to meet requirements of the most recent vehicle emissions standards (e.g. ARB/US EPA, China 6, Euro 6) [6,7]. Various other particulate sensing technologies for the exhaust system OBD have been reported. A radio frequency (RF) detector utilizes antenna probes inserted in the DPF housing to monitor RF signal attenuation and frequency shift caused by soot build-up in the filter [8,9]. The electrostatic sensor consists of a pair of isolated electrodes inserted into the PM stream [10,11]. A high electric field of approximately 500 V/mm is applied between them causing some of the charged particles to be deflected towards the electrodes resulting in a measurable leakage current on the order of few nA [12,13]. Optical soot detection methods, based on laser beam scattering or laser induced incandescence have also been previously demonstrated [14,15]. While these technologies can continuously monitor PM concentrations, they require a rather complex signal generation and readout circuitry, a

\* Corresponding author at: School of Microelectronics, Southern University of Science and Technology (SUSTech), Shenzhen 518055, China.

E-mail address: [yuh@ustech.edu.cn](mailto:yuh@ustech.edu.cn) (H. Yu).

voltage bias on the order of 1–2 kV or costly optoelectronic components. The conductometric sensor was developed as low-cost solution for exhaust soot measurements. It consists of a pair of interdigitated Pt electrodes formed on an insulating ceramic substrate and a resistive heater on the backside [16,17]. A polarization voltage is applied between the electrodes promoting soot accumulation on the surface by electrophoresis [18]. Resistance decreases with soot accumulation as conductive dendritic bridges gradually connect the electrodes. Once a certain current level is detected, the sensor is regenerated by heating to 600 °C. This sensor cannot continuously monitor soot concentration as an accumulation period, known as dead-band, is required to form the first conductive paths, which depends on the applied voltage, electrode spacing and soot concentration [19,20]. Several modifications have been proposed to shorten this percolation time [7,21,22].

Field effect devices such as Schottky diodes and transistors fabricated using chemically stable wide bandgap semiconductors such as silicon carbide (SiC) and gallium nitride (GaN) have been demonstrated for a wide range for gas and chemical sensors operated at high-temperature and harsh environments [23–26]. Previous reports for automotive applications mostly focused on the measurement of exhaust gases such as NH<sub>3</sub>, NO<sub>x</sub>, CO, and hydrocarbons [27–30], while only few studies considered PM detection. A SiC MOSFET soot detector with a floating gate in a low temperature co-fired ceramic package was reported by Sobocinski et al. [31]. A back-to-back Pt-GaN Schottky diode with interdigitated electrode design was also demonstrated for PM detection [32]. Both devices demonstrated near-instantaneous response.

In this article, we fabricated and demonstrated the applicability of a highly miniaturized and low complexity gateless AlGaN/GaN high electron mobility transistor (HEMT) to detect diesel soot particulate matter. The response to increasing amount of charged soot loading was characterized and the detection mechanism was presented. The response time, magnitude, and signal saturation as well as the ability of the device to withstand thermal regeneration process at 600 °C was examined.

## 2. Experimental

### 2.1. Sensor fabrication process

The devices were fabricated using well-established semiconductor fabrication processes on a commercially available epitaxial structure used for AlGaN/GaN HEMT fabrication. It was grown by metal organic chemical vapor deposition (MOCVD) on 2-in. sapphire substrate starting with a proprietary nucleation layer, followed by 1.5 μm Fe-doped GaN buffer, 300 nm undoped GaN channel, 1 nm AlN interlayer, an undoped 21 nm Al<sub>0.26</sub>Ga<sub>0.74</sub>N barrier and undoped 1.5 nm GaN capping layer. Strong polarization effects at the AlGaN/GaN heterojunction form a triangular quantum well filled with high mobility electrons, the two-dimensional electron gas (2DEG), which is utilized as the high carrier density channel of typical HEMTs [33].

The sensor micro-fabrication started with 100 nm deep inductively coupled plasma (ICP) etching of the epi to define individual devices. Afterwards, substrate cleaning was done using 3:1/H<sub>2</sub>SO<sub>4</sub>:H<sub>2</sub>O<sub>2</sub> solution, acetone, isopropanol, and DI water. Metal contact patterns were then formed by optical photolithography followed by a 60 s dip in 1:4/HCl:H<sub>2</sub>O solution to etch the native surface oxide. Immediately after, a multilayer metal contact stack consisting of Ti/Al/Ti/Au with thickness of 20/110/40/50 nm, was deposited by e-beam evaporation and patterned by lift-off. To form ohmic contacts to the 2DEG rapid thermal annealing was done at 850 °C for 45 s in N<sub>2</sub> ambient. Then a second metallization layer of 20/300 nm Ti/Au was evaporated and lift-off patterned for probing and wire-bonding. Finally, 200 nm of PECVD SiN<sub>x</sub> were deposited to passivate the contacts. It was then etched by a combination of reactive ion etching (RIE) and buffered oxide etchant (BOE) to expose the sensing area and probing pads. The dimensions of the sensing area opening were 40 μm × 400 μm and source-drain spacing was 60 μm. The schematic cross-section of the fabricated device and top

view image are shown in Fig. 1.

### 2.2. Testing of sensors

The processed wafers were cut by laser scribing into individual devices for testing. The schematic representation of the constructed PM testing setup is shown in Fig. 2. The soot particulates were generated by a laminar non-premixed flame, using a wick burner and commercial diesel as fuel. The cotton wick diameter and height above the nozzle were 5 and 7 mm, respectively. The burner was placed inside a 20 L glass container and synthetic air (O<sub>2</sub>/N<sub>2</sub> = 21%/79%) was supplied through a hole at the bottom with the airflow adjusted to 7 L/min using a flowmeter to maintain a steadily sooting flame. An inverted glass funnel with spout inner diameter of 14 mm was fitted on the top to form a narrow soot exhaust, where the test samples were inserted. To determine the particulate deposition rate of our setup, 0.6 × 0.6 cm<sup>2</sup> Si chips were exposed to the particle stream with increasing duration and their weight was measured using a microbalance with 1 μg readability (XPR2, Mettler-Toledo). Raman spectra of the deposited diesel soot were obtained using LabRAM HR evolution (Horiba) spectrometer with 532 nm excitation wavelength. Thermogravimetric analysis (TGA) instrument (Discovery TGA, TA Instruments) was utilized to determine the soot oxidation temperature and to perform sensor regeneration experiments. The tested sensors were mounted on Si chips and then inserted into the funnel spout perpendicular to the particle flow direction. Electrical sensor response signals were measured using a 4200-SCS semiconductor parameter analyzer (Keithley Instruments).

## 3. Results and discussion

The PM mass concentration was first estimated to be approximately 14 mg/m<sup>3</sup> by gravimetric method using paper filters [34]. This value is in the range of those produced by diesel engines with 2–2.2 L displacement [22,35]. The PM deposition rate on Si chips was then tested with increasing exposure time from 5 to 30 min. The particle mass was determined by comparing the mass of the samples before and after deposition using the microbalance. As shown in Fig. 3, a linear increase in PM mass was observed, therefore a stable and reproducible deposition rate of 0.25 μg/min or 0.69 μg/(cm<sup>2</sup> × min), when normalized to the surface area of the Si test chip, was obtained. The Raman spectrum scan of the produced diesel flame soot over the 1000–2000 cm<sup>-1</sup> frequency range is shown in Fig. 4a. It consists of two broad overlapping peaks and was obtained by averaging the results of 5 measurements at random locations across the sample and normalizing with respect to the G peak. The D peak at 1348 cm<sup>-1</sup> originates from defects at the edges of the graphitic crystallites and the G peak at 1594 cm<sup>-1</sup> arises from ideal sp<sup>2</sup>-bonded crystalline graphite. The peak positions correspond well to previously reported results on Raman analysis of diesel soot [36,37]. A mass loss curve for 8 mg of soot obtained from TGA experiments is shown in Fig. 4b. The oxidation intensified at 550 °C, where a 10% weight reduction was observed and then proceeded rapidly with 85% of particulates oxidized at 700 °C.

The PM sensing capability of the fabricated gateless AlGaN/GaN-HEMT sensors was studied by measuring the changes of the output characteristics i.e. drain current versus drain-source voltage ( $I_{DS}$ - $V_{DS}$ ) with increasing particle deposition time, as shown in Fig. 5a. The  $I$ - $V$  characteristics of the gateless device still demonstrate the linear and saturation regions, similarly to gated HEMTs. Under the assumption that the electron sheet density ( $n_s$ ) across the 2DEG channel is constant the drain current in the linear regime can be estimated according to:

$$I_{DS,lin} = en_s\mu W_{ch}V_{DS}/L_{ch} = en_s\mu W_{ch}E_{ch} \quad (1)$$

where  $e$  is the electron charge,  $\mu$  is the low field electron mobility,  $W_{ch}$  is the width of the channel,  $L_{ch}$  is the source-drain spacing, and  $E_{ch}$  is the channel electric field. With increasing  $V_{DS}$ , the critical value of the

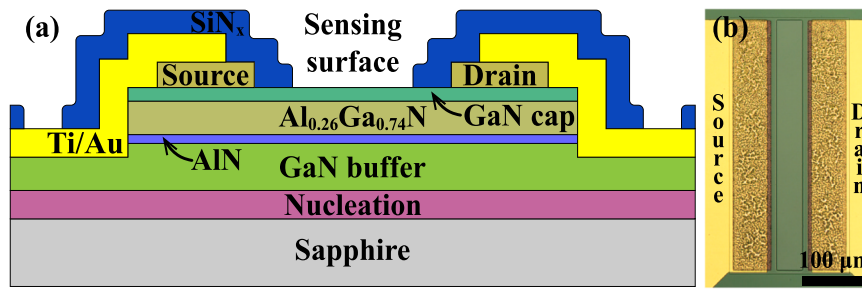


Fig. 1. Schematic cross-section (a) and top-view micrograph (b) of the fabricated PM sensor.

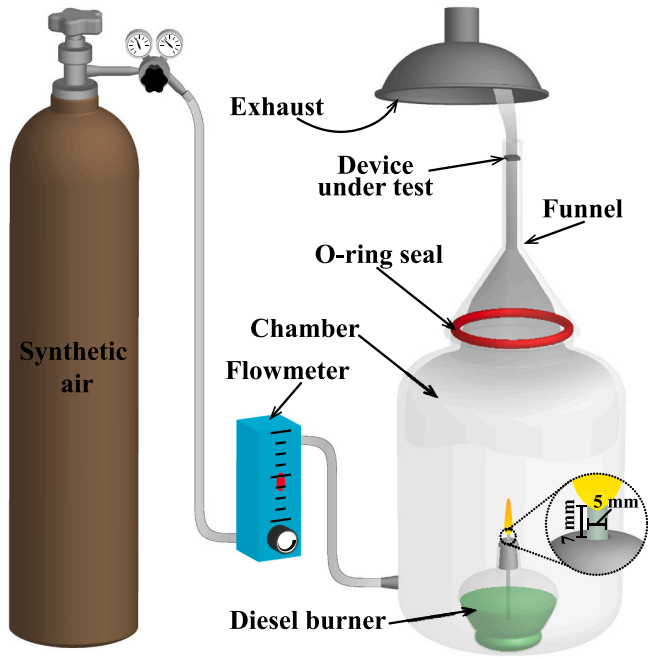


Fig. 2. Schematic illustration of the experimental setup used for soot deposition.

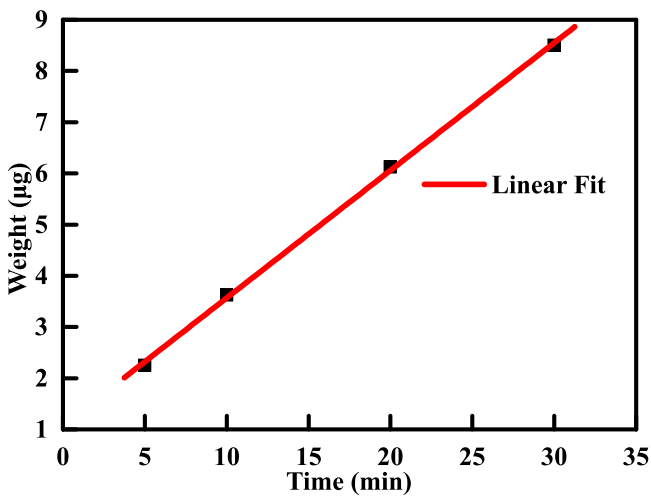


Fig. 3. Measured soot particle mass with increasing deposition time.

electric field ( $E_{cr}$ ) is reached  $E_{ch} \geq E_{cr} = v_{sat}/\mu$  at which point the channel electron velocity ( $v_{sat}$ ) and drain current ( $I_{DS,sat}$ ) saturate [38]:

$$I_{DS,sat} = en_s \mu W_{ch} E_{cr} = en_s W_{ch} v_{sat} \quad (2)$$

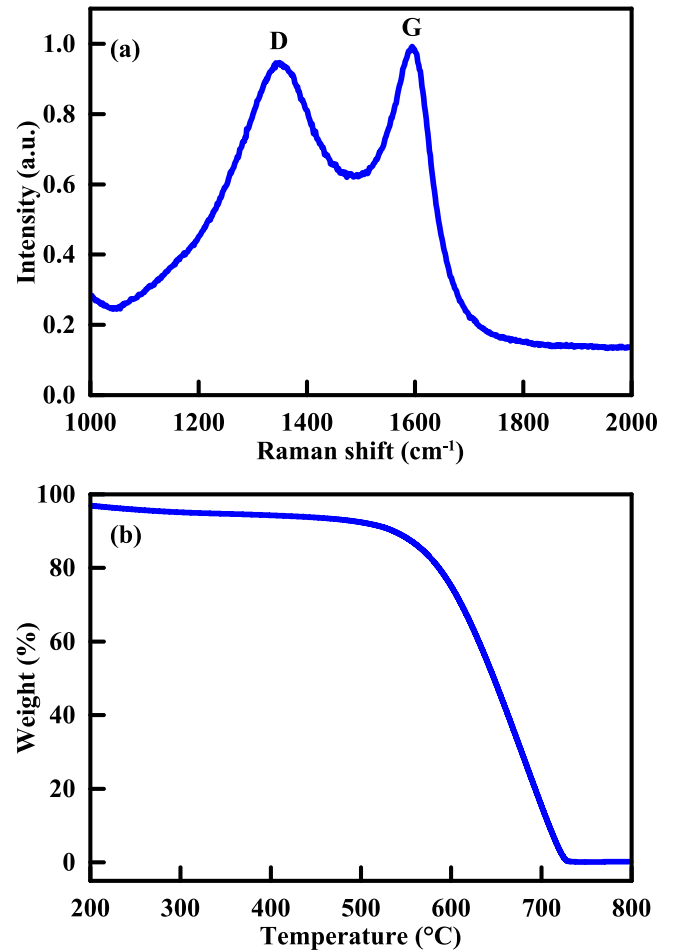
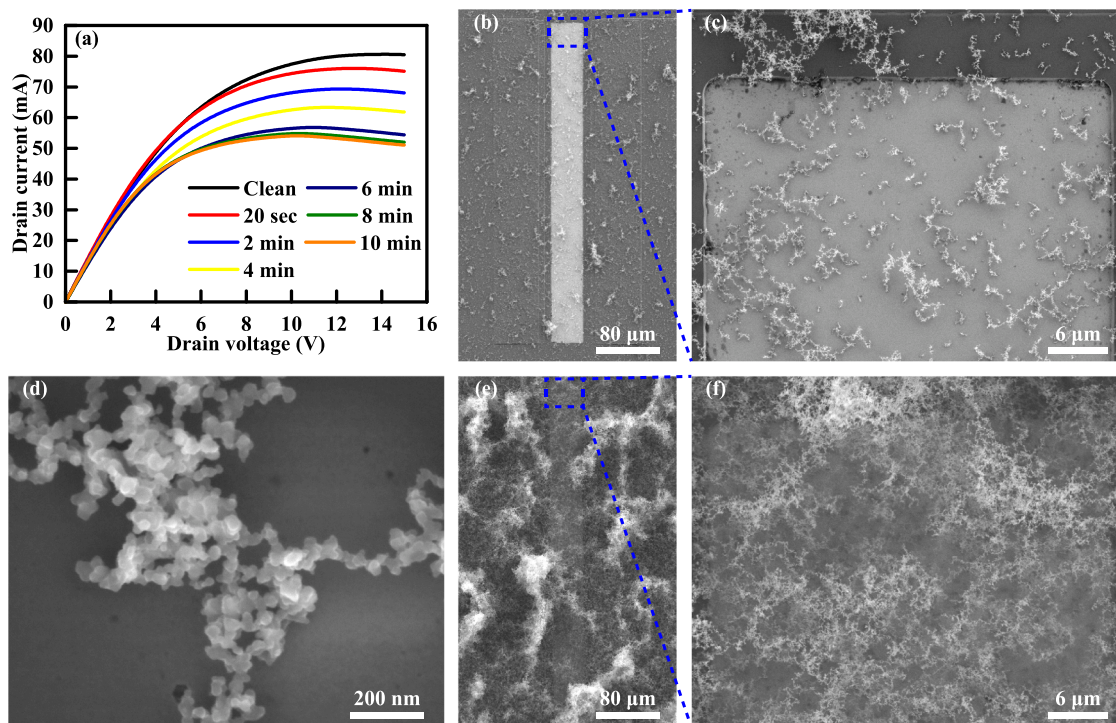


Fig. 4. Raman spectrum (a) and TGA profile (b) of diesel soot produced by laminar flame using a wick burner.

The output current ( $I_{DS,sat}$ ) decreased by 4.4 mA at  $V_{DS} = 13$  V after just 20 s of PM exposure. The corresponding scanning electron microscope (SEM) images of the sensing area are shown in Fig. 5b and c. After 20 s of deposition only sparsely distributed dendritic soot agglomerates were observed on the sensing area (Fig. 5c). The estimated average particle diameter was  $31 \pm 5$  nm, as shown in Fig. 5d. The  $I_{DS,sat}$  continued to gradually reduce up to 8 min of total deposition time, after which signal saturation was observed. The sensing surface was completely covered by a continuous layer of soot after 10 min as shown in Fig. 5e and f. The performance of our device was further characterized by determining the absolute sensing response ( $S$ ), defined as:

$$S(\%) = \left| \frac{I_{DS,PM} - I_{DS,CL}}{I_{DS,CL}} \right| \times 100\% = \left| \frac{\Delta I_{DS}}{I_{DS,CL}} \right| \times 100\% \quad (3)$$



**Fig. 5.** Output characteristics ( $I_{DS}$ – $V_{DS}$ ) of the gateless AlGaIn/GaN HEMT soot sensor with increasing particle deposition time (a). SEM images of the sensor surface after 20 s of deposition (b), (c). High magnification image of agglomerated soot particles (d). SEM images of the sensor surface after 10 min of deposition (e), (f).

where  $I_{DS,CL}$  and  $I_{DS,PM}$  is the drain current magnitude of the clean and PM-exposed sensor, respectively. Fig. 6 shows the sensing response variation with increasing soot deposition time. Evidently, the response increased from 5.52% after 20 s to 34.72% after 10 min of deposition time. Table 1 presents the PM mass deposited on the sensing surface, estimated from earlier microbalance experiments (see Fig. 3), during the tested exposure times as well as the corresponding  $S$  and signal variation ( $\Delta I_{DS}$ ). The high values of  $S$  and  $\Delta I_{DS}$  are attributed to the signal amplification property of the gateless-HEMT as the 2DEG density is exceptionally sensitive to variations in surface potential caused by adsorption of charged particulates [26,30].

In order to better explain the PM sensing mechanism, the formation of the 2DEG in the AlGaIn/GaN heterostructure is summarized first. GaN has a wurtzite crystal structure with non-ideal hexagonal close-packed

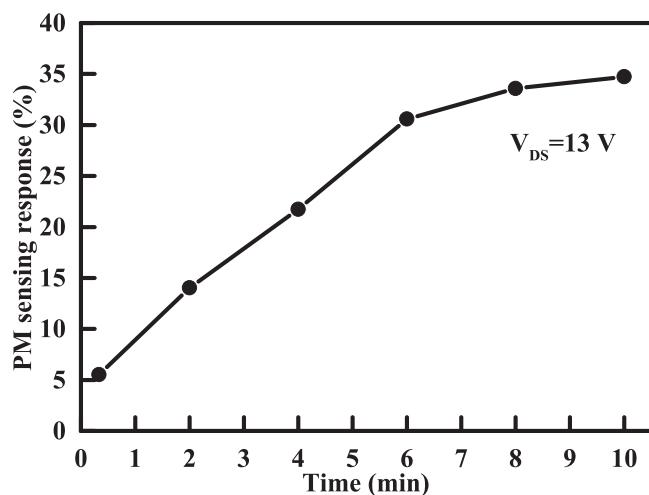


**Fig. 6.** Particulate matter sensing response with increasing deposition time at  $V_{DS} = 13$  V.

**Table 1**

Estimated PM mass on the sensing surface with increasing deposition time, the corresponding sensing response ( $S$ ), and signal variation ( $\Delta I_{DS}$ ).

Time (min)	PM mass (ng)	$S$ (%)	$\Delta I_{DS}$ (mA)
1/3	0.04	5.52	4.44
2	0.22	14.02	11.28
4	0.44	21.72	17.47
6	0.66	30.57	24.60
8	0.88	33.59	27.03
10	1.10	34.72	27.94

arrangements lacking inversion symmetry. Additionally, the difference in electronegativities of III–N bonds is high, resulting in the largest spontaneous polarization ( $P_{SP}$ ) among III–V semiconductors [39]. When a thin layer of wider bandgap AlGaIn is pseudomorphically grown on GaN it is under tensile strain giving rise to additional piezoelectric polarization ( $P_{PZ}$ ) in the same direction as  $P_{SP}$ . The difference in total polarization between AlGaIn and GaN induces a positive sheet charge at the interface on the AlGaIn side and a negative charge at the surface. Free electrons are then attracted to the interface and confined in the triangular quantum well, the 2DEG, at the interface on the GaN side [40]. As the AlGaIn/GaN heterojunction is not doped, previous studies had indicated that the 2DEG electrons are supplied from donor-like surface states present at the surface of the AlGaIn barrier and the thin GaN cap layer. The released electrons are swept to the heterojunction interface by the strong polarization induced electric field, while the positively charged donors on the surface ensure overall charge neutrality across the barrier [41–43]. The thin AlN layer, grown between AlGaIn and GaN channel, is known to enhance the 2DEG density and mobility, while the top GaN cap increases the effective Schottky barrier of standard HEMTs with a gate electrode [44,45]. Additionally, having the epitaxial structure terminated with GaN improves the stability of the sensing surface by mitigating the thermal oxidation of AlGaIn [46]. Adsorption of charged species can alter the potential distribution on the GaN/AlGaIn surface. The observed reduction in drain

current indicates that some of the surface states get neutralized by the PM as schematically demonstrated in Fig. 7a. Conduction band diagrams illustrating the partial depletion of the 2DEG due to PM adsorption on the sensing area are shown in Fig. 7b. This suggests that either more negatively than positively charged particles are produced from diesel flame under our testing conditions or that negative particles are preferentially attracted by the charged surface states. Furthermore, previously reported experiments of ungated AlGaIn/GaN HEMT exposure to ionized air demonstrated that negative ion adsorption resulted in significant reduction in drain current, while positive ions caused the current to increase [47]. The proposed mechanism of our sensor differs from the reported in [32] for a back-to-back Pt-GaN Schottky device, where particle adsorption on the lateral extension of the depletion region at the Pt-GaN interface resulted in increased reverse bias current due to Schottky barrier lowering. The estimated lateral depletion width was on the order of 50–100 nm, therefore interdigitated design, and increased dimensions ( $1 \times 1 \text{ cm}^2$ ) were required in order to enhance the

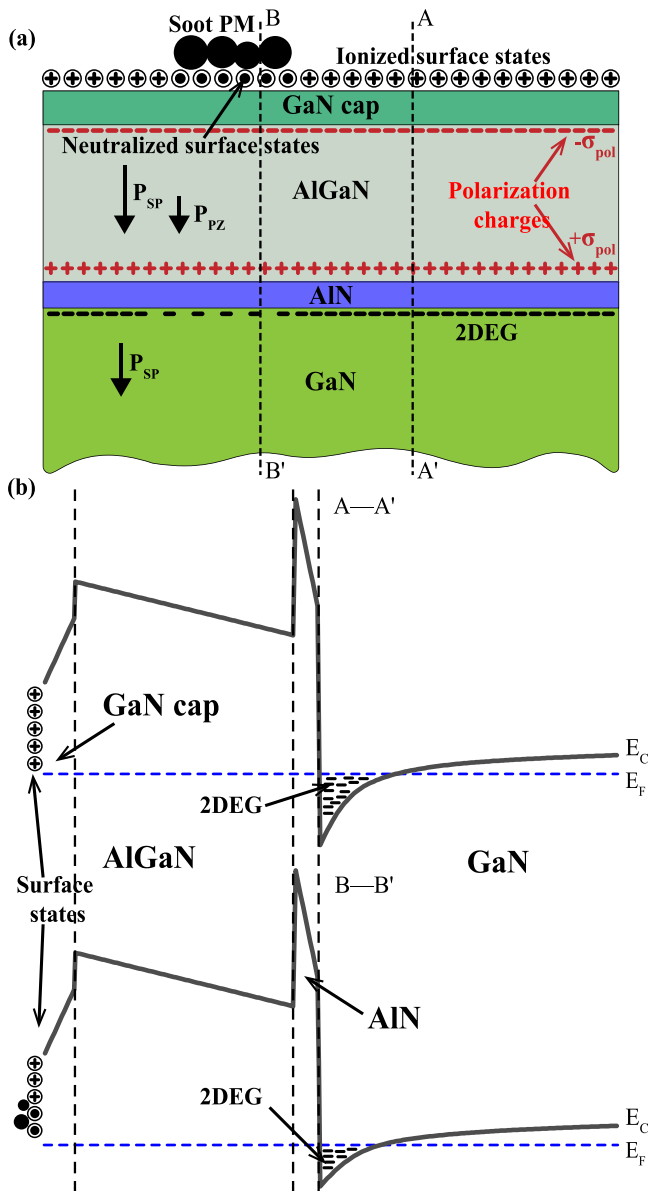


Fig. 7. (a) Schematic diagram of the AlGaIn/GaN heterostructure indicating the direction of  $P_{SP}$ ,  $P_{PZ}$  and the position of the resulting charges. (b) Conduction band diagrams of the sensor with clean surface (line A—A') and with adsorbed soot (line B—B').

sensor response [32].

To investigate the regeneration ability of the developed sensor, soot was deposited for 10 min and the chip was heated from room temperature to  $600 \text{ }^\circ\text{C}$  at  $50 \text{ }^\circ\text{C}/\text{min}$  and held for 10 min using the TGA system. Optical micrographs of the clean, PM-coated, and regenerated sensing area are shown in Fig. 8a–c. It is evident that the particles were successfully oxidized and removed from the sensing surface (Fig. 8c). Comparing a fresh and thermally regenerated device it was observed that the surface roughness of the interconnect (IC) metal increased due to the interdiffusion of Ti and Au as evident from Fig. 8d and e. Some cracks in the  $\text{SiN}_x$  have also appeared on top of the metallization. The  $I$ - $V$  characteristics of the sensor response to 10 min soot exposure before and after the recovery cycle are shown in Fig. 9a. The electrical properties remained almost unchanged after regeneration and the sensing response of approximately 31% at  $V_{DS} = 13 \text{ V}$  was maintained. It was observed that the on-resistance ( $R_{ON}$ ), extracted from the slope of the linear region of the  $I$ - $V$  curve (red and orange dashed lines in Fig. 9a), increased from 71 to  $103 \text{ }\Omega$  after regeneration. The total  $R_{ON}$  of our gateless HEMT sensor is expressed as:

$$R_{ON} = R_{2DEG} + 2R_C + 2R_M \quad (4)$$

where  $R_{2DEG}$  is the resistance of the 2DEG channel,  $R_C$  is the contact resistance of the source/drain electrodes and  $R_M$  is the metal IC resistance. In order to determine the reason for the  $R_{ON}$  increase after the regeneration cycle, each of the variables of Eq. (4) was extracted separately. The sheet resistance ( $R_{sh,2DEG}$ ) of the 2DEG channel and  $R_C$  were measured using circular transmission line model (CTLM) test structures [48], while the sheet resistance of the interconnect metallization ( $R_{sh,M}$ ) was measured using Greek cross test structures [49], which were included in the photo-lithography masks of the PM sensors. After measuring the sheet resistances, the  $R_{2DEG}$  and  $R_M$  can be calculated as:

$$R_{2DEG} = \frac{L_{ch}}{W_{ch}} R_{sh,2DEG} \quad (5)$$

$$R_M = \frac{L_M}{W_M} R_{sh,M} \quad (6)$$

where  $W_M$  and  $L_M$  are the width and length of the IC metal lines, respectively. The parameters measured from the test structures before and after the regeneration cycle are summarized in Table 2. It is evident that the heterojunction characteristics (the 2DEG) did not deteriorate due to the wide-bandgap and high temperature tolerance of GaN and AlGaIn. An earlier study on the effects of annealing AlGaIn/GaN at  $600 \text{ }^\circ\text{C}$  for 5 h in air demonstrated that unpassivated surface with GaN cap layer (equivalent to the sensing surface of our PM sensor) had less degraded electrical properties when compared to the same structure passivated with  $\text{Al}_2\text{O}_3$  [50]. The metal-semiconductor ohmic contact resistance also did not change significantly. Previous reports have shown that high-temperature annealed contacts to GaN and AlGaIn/GaN with a multilayer metal structure remained stable after several hours of thermal aging at  $600 \text{ }^\circ\text{C}$  [51–53]. On the other hand, the sheet resistance of the interconnect metallization increased almost 15 times. Interdiffusion of Ti and Au is known to occur at temperatures above  $200 \text{ }^\circ\text{C}$  leading to the formation of intermetallic compounds and increased resistance of the bilayer film [54,55]. The calculated  $R_{ON}$  before and after regeneration using the parameters in Table 2 and considering sensor dimensions were 68 and  $107 \text{ }\Omega$ . These results correlate well with the values extracted from  $I$ - $V$  measurements (Fig. 9a). Additional regeneration test cycles were then conducted. The sensing response towards 10 min soot deposition ( $V_{DS} = 13 \text{ V}$ ) and on-resistance measurement results are shown in Fig. 9b. It was observed that  $R_{ON}$  did not increase further after the added thermal cycles and the PM response was maintained in the 26–30% range. However, after the 5th cycle some of the IC pads delaminated as shown in the inset of Fig. 9b. The adhesion degradation is also due to the diffusion Ti into Au as well as stress caused

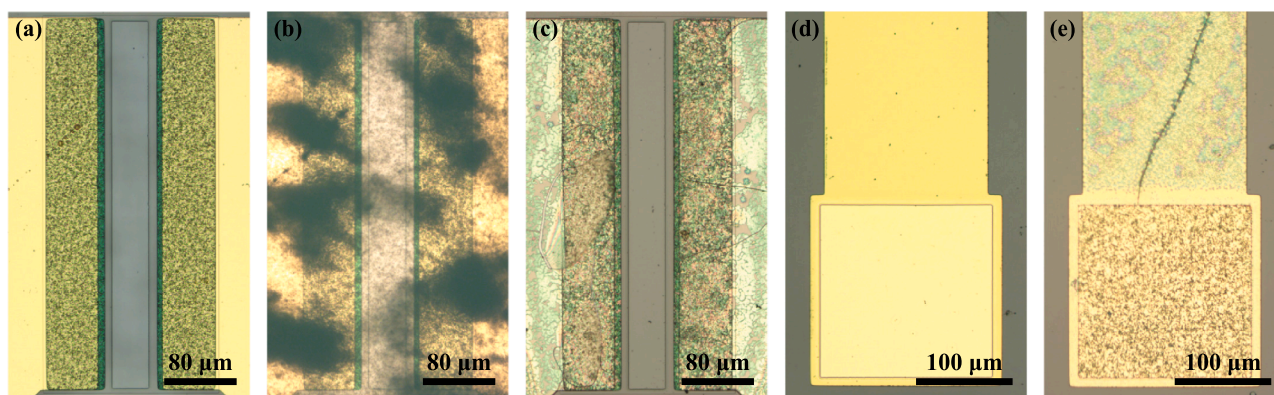


Fig. 8. Optical micrographs of the sensing area before (a), after (b) PM deposition and after thermal regeneration at 600 °C (c). Surface of the interconnect metallization before (d) and after (e) thermal regeneration at 600 °C.

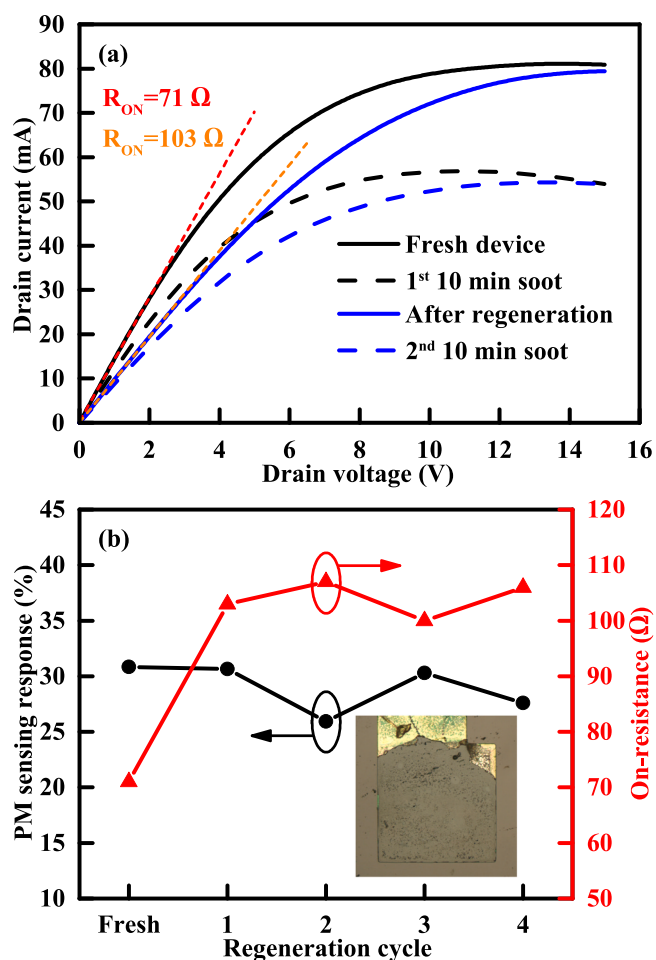


Fig. 9. (a) Output characteristics ( $I_{DS}-V_{DS}$ ) of the gateless AlGaN/GaN HEMT soot sensor before and after thermal regeneration at 600 °C. (b) Sensing response at  $V_{DS} = 13$  V and on-resistance variation after additional regeneration cycles. The inset depicts IC delamination observed after the 5th regeneration cycle.

by mismatch of thermal expansion coefficient between the metal and the substrate. Therefore, the gateless HEMT diesel soot sensor can withstand the thermal regeneration cycle, however the IC metallization requires further optimization to prevent the increase of  $R_M$  and delamination. Inserting a diffusion barrier such as TiN or Pt between Ti and Au would limit thermal interdiffusion or a different metallization may be utilized

Table 2

Resistance parameters measured on dedicated test structures before and after thermal regeneration at 600 °C.

Parameter	Fresh device	Post-regeneration
$R_C$ ( $\Omega$ mm)	0.97	1.08
$R_{sh,2DEG}$ ( $\Omega$ /sq)	397	370
$R_{sh,M}$ ( $\Omega$ /sq)	0.074	1.08

[55,56].

To perform in-situ regeneration inside the exhaust system the proposed sensor can be micro-fabricated to include a resistive micro-heater and temperature sensor, similarly to a previously demonstrated NO<sub>2</sub> sensor [57]. Additionally, monitoring of emitted pollutant gases can be achieved by integrating other HEMT-based sensors on the same chip [24,30].

#### 4. Conclusions

In this work, a gateless AlGaN/GaN HEMT micro-sensor was fabricated and tested for the detection of diesel particulate matter emissions. An in-house testing setup was assembled to produce soot particles from laminar diesel flame with an estimated mass concentration of 14 mg/m<sup>3</sup> and surface deposition rate of 0.25  $\mu$ g/min. The adsorption of PM on the exposed semiconductor surface between source/drain electrodes resulted in measurable reduction of 2DEG channel current, due to the neutralization of positive surface states by negatively charged particulates. Exposure of only 20 s resulted in signal response of 5.5% or 4.4 mA, which indicates that there was essentially no dead-band period. The highest response when signal saturation occurred was 34.72% (27.94 mA) obtained after 10 min of deposition due to the sensing surface being fully covered by PM. Afterwards, the sensor was successfully regenerated at 600 °C in air and was still operational without degradation of 2DEG current, contact resistance and PM sensing response. The observed increase of on-resistance was studied and attributed to the Ti-Au interdiffusion of interconnect metallization, which also led to delamination after several regeneration cycles. Based on these findings, the AlGaN/GaN HEMT soot sensor is an interesting alternative technology for on-board diagnostics of automotive exhaust systems, that is also compatible with on-chip integration of micro-heaters and temperature sensors for rapid regeneration as well as field-effect based detectors of other pollutant gases. In addition, processing optimizations are still required to resolve the observed interconnect reliability problems after thermal regeneration.

## CRedit authorship contribution statement

**Robert Sokolovskij:** Conceptualization, Methodology, Investigation, Validation, Writing – original draft. **Hongze Zheng:** Investigation, Resources. **Wenmao Li:** Investigation, Visualization. **Guangan Zhou:** Investigation, Formal analysis. **Qing Wang:** Resources, Project administration. **Guoqi Zhang:** Supervision, Validation. **Hongyu Yu:** Supervision, Validation, Funding acquisition.

## Declaration of Competing Interest

The authors declare that they have no known competing financial interests or personal relationships that could have appeared to influence the work reported in this paper.

## Acknowledgments

The funding for this research was provided by the Key-Area Research and Development Program of Guangdong Province projects “Research and application of key technologies of GaN-based power devices on Si substrate” (Grant no. 2019B010128001) and “Research on key technologies for optimization of IoT chips and product development” (Grant no. 2019B010142001) and the Shenzhen Municipal Council of Science and Innovation (Grant Nos. JCYJ20170412153356899, JCYJ20210324120409025 and JCYJ20200109141233476). This work was conducted at SUSTech Core Research Facilities (CRF) and we would like to acknowledge the technical support from SUSTech CRF staff and engineers.

## References

- H.A. Michelsen, M.B. Colket, P.-E. Bengtsson, A. D’Anna, P. Desgroux, B.S. Haynes, J.H. Miller, G.J. Nathan, H. Pitsch, H. Wang, A review of terminology used to describe soot formation and evolution under combustion and pyrolytic conditions, *ACS Nano* 14 (2020) 12470–12490, <https://doi.org/10.1021/acsnano.0c06226>.
- A. Kurniawan, A. Schmidt-Ott, Monitoring the soot emissions of passing cars, *Environ. Sci. Technol.* 40 (2006) 1911–1915, <https://doi.org/10.1021/es051140h>.
- D. Tang, R. Zhao, S. Wang, J. Wang, L. Ni, L. Chen, The simulation and experimental research of particulate matter sensor on diesel engine with diesel particulate filter, *Sens. Actuators A* 259 (2017) 160–170, <https://doi.org/10.1016/j.sna.2017.03.036>.
- T. Kamimoto, A review of soot sensors considered for onboard diagnostics application, *Int. J. Engine Res.* 18 (2017) 631–641, <https://doi.org/10.1177/1468087416678499>.
- B. Guan, Z. Reggie, L. He, Z. Huang, Review of the state-of-the-art of exhaust particulate filter technology in internal combustion engines, *J. Environ. Manag.* 154 (2015) 225–258, <https://doi.org/10.1016/j.jenvman.2015.02.027>.
- H. Husted, G. Roth, S. Nelson, L. Hocken, G. Fulks, D. Racine, Sensing of particulate matter for on-board diagnosis of particulate filters, *SAE Int. J. Engines* 5 (2012) 235–247, <https://doi.org/10.4271/2012-01-0372>.
- A. Kondo, S. Yokoi, T. Sakurai, S. Nishikawa, T. Egami, M. Tokuda, T. Sakuma, New particulate matter sensor for on board diagnosis, *SAE Int. J. Engines* 4 (2011) 117–125, <https://doi.org/10.4271/2011-01-0302>.
- A. Sappok, P. Ragaller, L. Bromberg, V. Prikhodko, J. Storey, J. Parks, Real-Time Engine and After Treatment System Control Using Fast Response Particulate Filter Sensors (SAE Technical Paper 2016-01-0918), 2016, <https://doi.org/10.4271/2016-01-0918>.
- H. Najundaswamy, V. Nagaraju, Y. Wu, E. Kochler, A. Sappok, P. Ragaller, L. Bromberg, Advanced RF Particulate Filter Sensing and Controls for Efficient after Treatment Management and Reduced Fuel Consumption (SAE Paper 2015-01-0996), 2015, <https://doi.org/10.4271/2015-01-0996>.
- M. Maricq, On the electrical charge of motor vehicle exhaust particles, *Aerosol Sci.* 37 (2006) 858–874, <https://doi.org/10.1016/j.jaerosci.2005.08.003>.
- A. Warey, B. Hendrix, M. Hall, T. Nevius, A New Sensor for On-Board Detection of Particulate Carbon Mass Emissions from Engines (SAE Technical Paper 2004-01-2906), 2004, <https://doi.org/10.4271/2004-01-2906>.
- G. Hauser, Smoke Particulate Sensors for OBD and High Precision Measuring (SAE Technical Paper 2006-01-3549), 2006, <https://doi.org/10.4271/2006-01-3549>.
- D. Bilby, D. Kubinski, M. Maricq, Current amplification in an electrostatic trap by soot dendrite growth and fragmentation: application to soot sensors, *Aerosol Sci.* 98 (2016) 41–58, <https://doi.org/10.1016/j.jaerosci.2016.03.003>.
- T. Kamimoto, Y. Murayama, T. Minagawa, T. Minami, Light scattering technique for estimating soot mass loading in diesel particulate filters, *Int. J. Engine Res.* 10 (2009) 323–336, <https://doi.org/10.1243/14680874JER03109>.
- Z. Zhang, L. del Re, R. Fuerhapter, Fast Hybrid Sensor for Soot of Production CI Engines (SAE Technical Paper 2017-24-0137), 2017, <https://doi.org/10.4271/2017-24-0137>.
- T. Ochs, H. Schittenhelm, A. Genssle, B. Kamp, Particulate matter sensor for onboard diagnostics (OBD) of diesel particulate filters (DPF), *SAE Int. J. Fuels Lubr.* 3 (2010) 61–69, <https://doi.org/10.4271/2010-01-0307>.
- G. Hagen, C. Feistkorn, S. Wiegärtner, A. Heinrich, D. Brüggemann, R. Moos, Conductometric soot sensor for automotive exhausts: initial studies, *Sensors* 10 (2010) 1589–1598, <https://doi.org/10.3390/s100301589>.
- G. Hagen, C. Spannauer, M. Feulner, J. Kita, A. Müller, R. Moos, Conductometric soot sensors: internally caused thermophoresis as an important undesired side effect, *Sensors* 18 (10) (2018) 3531, <https://doi.org/10.3390/s18103531>.
- P. Fragkiadoulakis, S. Geivanidis, Z. Samaras, Modeling a resistive soot sensor by particle deposition mechanisms, *J. Aerosol Sci.* 123 (2018) 76–90, <https://doi.org/10.1016/j.jaerosci.2018.06.005>.
- D. Grondin, P. Breuil, J.P. Viricelle, P. Vernoux, Modeling of the signal of a resistive soot sensor, influence of the soot nature and of the polarization voltage, *Sens. Actuators B: Chem.* 298 (2019), 126820, <https://doi.org/10.1016/j.snb.2019.126820>.
- P. Bartscherer, R. Moos, Improvement of the sensitivity of a conductometric soot sensor by adding a conductive cover layer, *J. Sens. Sens. Syst.* 2 (2013) 95–102, <https://doi.org/10.5194/jsss-2-95-2013>.
- G. Hagen, M. Feulner, R. Werner, M. Schubert, A. Müller, G. Rieß, D. Brüggemann, R. Moos, Capacitive soot sensor for diesel exhausts, *Sens. Actuators B: Chem.* 236 (2016) 1020–1027, <https://doi.org/10.1016/j.snb.2016.05.006>.
- M. Andersson, R. Pearce, A. Lloyd Spetz, New generation SiC based field effect transistor gas sensors, *Sens. Actuators B Chem.* 179 (2013) 95–106, <https://doi.org/10.1016/j.snb.2012.12.059>.
- R. Sokolovskij, J. Zhang, E. Iervolino, C. Zhao, F. Santagata, F. Wang, H. Yu, P. M. Sarro, Q.G. Zhang, Hydrogen sulfide detection properties of Pt-gatedAlGaN/GaN HEMT-sensor, *Sens. Actuators B: Chem.* 274 (2018) 636–644, <https://doi.org/10.1016/j.snb.2018.08.015>.
- N. Chaniotakis, N. Sofikiti, Novel semiconductor materials for the development of chemical sensors and biosensors: a review, *Anal. Chim. Acta* 615 (2008) 1–9, <https://doi.org/10.1016/j.aca.2008.03.046>.
- K.T. Upadhyay, M.K. Chattopadhyay, Sensor applications based on AlGaN/GaN heterostructures, *Mater. Sci. Eng.: B* 263 (2021), 114849, <https://doi.org/10.1016/j.mseb.2020.114849>.
- M. Andersson, P. Ljung, M. Mattsson, M. Löfdahl, A. Lloyd Spetz, Investigations on the possibilities of a MISiCFET sensor system for OBD and combustion control utilizing different catalytic gate materials, *Top. Catal.* 30–31 (2004) 365–368, <https://doi.org/10.1023/B:TOCA.0000029776.18603.74>.
- H. Wingbrant, H. Svenningstorp, P. Salomonsson, D. Kubinski, J.H. Visser, M. Löfdahl, A. Lloyd Spetz, Using a MISiC-FET sensor for detecting NH<sub>3</sub> in SCR systems, *IEEE Sens. J.* 5 (2005) 1099–1105, <https://doi.org/10.1109/JSEN.2005.854489>.
- N.G. Wright, A.B. Horsfall, SiC sensors: a review, *J. Phys. D Appl. Phys.* 40 (2007) 6345–6354, <https://doi.org/10.1088/0022-3727/40/20/S17>.
- Y. Halfaya, C. Bishop, A. Soltani, S. Sundaram, V. Aubry, P. Voss, J.-P. Salvestrini, A. Ougazzaden, Investigation of the performance of HEMT-based NO, NO<sub>2</sub> and NH<sub>3</sub> exhaust gas sensors for automotive antipollution systems, *Sensors* 16 (273) (2016), <https://doi.org/10.3390/s16030273>.
- M. Sobocinski, D. Bilby, D. Kubinski, J. Visser, M. Andersson, J. Juuti, A. Lloyd Spetz, H. Jantunen, SiC MOSFET soot sensor in a co-fired LTCC package, *Procedia Eng.* 168 (2016) 27–30, <https://doi.org/10.1016/j.proeng.2016.11.123>.
- H. So, M. Hou, S.R. Jain, J. Lim, D.G. Senesky, Interdigitated Pt-GaN Schottky interfaces for high-temperature soot-particulate sensing, *Appl. Surf. Sci.* 368 (2016) 104–109, <https://doi.org/10.1016/j.apsusc.2016.01.178>.
- O. Ambacher, J. Smart, J.R. Shealy, N.G. Weimann, K. Chu, M. Murphy, W. J. Schaff, L.F. Eastman, R. Dimitrov, L. Wittmer, M. Stutzmann, W. Rieger, J. Hilsenbeck, Two dimensional electron gases induced by spontaneous and piezoelectric polarization charges in N- and Ga-face AlGaN/GaN heterostructures, *J. Appl. Phys.* 85 (1999) 3222–3233, <https://doi.org/10.1063/1.369664>.
- B. Giechaskiel, E. Schiefer, W. Schindler, H. Axmann, C. Dardiotis, Overview of soot emission measurements instrumentation: from smoke and filter mass to particle number, *SAE Int. J. Engines* 6 (2013) 10–22, <https://doi.org/10.4271/2013-01-0138>.
- D.G. Kim, S.H. Yang, H.S. Kim, Development of the particulate matter sensor for diesel engine, *Int. J. Automot. Technol.* 20 (2019) 359–364, <https://doi.org/10.1007/s12239-019-0035-6>.
- M. Saffariour, L.-L. Tay, K.A. Thomson, G.J. Smallwood, B.T. Brem, L. Durдина, M. Johnson, Raman spectroscopy and TEM characterization of solid particulate matter emitted from soot generators and aircraft turbine engines, *Aerosol Sci. Technol.* 51 (2017) 518–531, <https://doi.org/10.1080/02786826.2016.1274368>.
- J. Schmid, B. Grob, R. Niessner, N.P. Ivleva, Multiwavelength Raman microspectroscopy for rapid prediction of soot oxidation reactivity, *Anal. Chem.* 83 (2011) 1173–1179, <https://doi.org/10.1021/aci102939w>.
- J. Kuzmik, S. Bychikhin, D. Pogany, C. Gaquière, E. Morvan, Current conduction and saturation mechanism in AlGaN/GaN ungated structures, *J. Appl. Phys.* 99 (12) (2006), 123720, <https://doi.org/10.1063/1.2207572>.
- C. Ren, Polarisation fields in III-nitrides: effects and control, *Mater. Sci. Technol.* 32 (2016) 418, <https://doi.org/10.1179/1743284715Y.0000000103>.
- O. Ambacher, B. Foutz, J. Smart, J.R. Shealy, N.G. Weimann, K. Chu, M. Murphy, A.J. Sierakowski, W.J. Schaff, L.F. Eastman, R. Dimitrov, A. Mitchell, M. Stutzmann, Two dimensional electron gases induced by spontaneous and piezoelectric polarization in undoped and doped AlGaN/GaN heterostructures, *J. Appl. Phys.* 87 (2000) 334–344, <https://doi.org/10.1063/1.371866>.
- J.P. Ibbetson, P.T. Fini, K.D. Ness, S.P. DenBaars, J.S. Speck, U.K. Mishra, Polarization effects, surface states, and the source of electrons in AlGaN/GaN

- heterostructure field effect transistors, *Appl. Phys. Lett.* 77 (2000) 250–252, <https://doi.org/10.1063/1.126940>.
- [42] G. Koley, M. Spencer, On the origin of the two-dimensional electron gas at the AlGaIn/GaN heterostructure interface, *Appl. Phys. Lett.* 86 (4) (2005), 042107, <https://doi.org/10.1063/1.1850600>.
- [43] S. Heikman, S. Keller, Y. Wu, J.S. Speck, S.P. DenBaars, U.K. Mishra, Polarization effects in AlGaIn/GaN and GaN/AlGaIn/GaN heterostructures, *J. Appl. Phys.* 93 (2003) 10114–10118, <https://doi.org/10.1063/1.1577222>.
- [44] L. Shen, S. Heikman, B. Moran, R. Coffie, N.Q. Zhang, D. Buttari, I.P. Smorchkova, S. Keller, S.P. DenBaars, U.K. Mishra, AlGaIn/AlN/GaN high-power microwave HEMT, *IEEE Electron Device Lett.* 22 (2001) 457–459, <https://doi.org/10.1109/55.954910>.
- [45] E.T. Yu, X.Z. Dang, L.S. Yu, D. Qiao, P.M. Asbeck, S.S. Lau, G.J. Sullivan, K. S. Boutros, J.M. Redwing, Schottky barrier engineering in III–V nitrides via the piezoelectric effect, *Appl. Phys. Lett.* 73 (1998) 1880–1882, <https://doi.org/10.1063/1.122312>.
- [46] Z. Xu, J. Wang, J. Liu, Ch Jin, Y. Cai, Z. Yang, M. Wang, M. Yu, B. Xie, W. Wu, X. Ma, J. Zhang, Y. Hao, Demonstration of normally-off recess-gated AlGaIn/GaN MOSFET using GaN cap layer as recess mask, *IEEE Electron Device Lett.* 35 (2014) 1197–1199, <https://doi.org/10.1109/LED.2014.2359986>.
- [47] R. Neuberger, G. Müller, M. Eickhoff, O. Ambacher, M. Stutzmann, Observation of ion-induced changes in the channel current of high electron mobility AlGaIn/GaN transistors (HEMT), *Mater. Sci. Eng.: B* 93 (2002) 143–146, [https://doi.org/10.1016/S0921-5107\(02\)00053-3](https://doi.org/10.1016/S0921-5107(02)00053-3).
- [48] J.H. Klootwijk, C.E. Timmering, Merits and limitations of circular TLM structures for contact resistance determination for novel III–V HBTs, in: *Proceedings of the 2004 International Conference on Microelectronic Test Structures*, 2004, pp. 247–52, (<https://doi.org/10.1109/ICMTS.2004.1309489>).
- [49] S. Enderling, C.L. Brown, S. Smith, M.H. Dicks, J.T.M. Stevenson, M. Mitkova, M. N. Kozicki, A.J. Walton, Sheet resistance measurement of non-standard cleanroom materials using suspended Greek cross test structures, *IEEE Trans. Semicond. Manuf.* 19 (2006) 2–9, <https://doi.org/10.1109/TSM.2005.863248>.
- [50] M. Hou, S.R. Jain, H. So, T.A. Heuser, X. Xu, A.J. Suria, D.G. Senesky, Degradation of 2DEG transport properties in GaN capped AlGaIn/GaN heterostructures at 600 °C in oxidizing and inert environments, *J. Appl. Phys.* 122 (2017), 195102, <https://doi.org/10.1063/1.5011178>.
- [51] D. Selvanathan, F.M. Mohammed, A. Tesfayesus, I. Adesida, Comparative study of Ti/Al/Mo/Au, Mo/Al/Mo/Au, and V/Al/Mo/Au ohmic contacts to AlGaIn/GaN heterostructures, *J. Vac. Sci. Technol. B* 22 (2004) 2409–2416, <https://doi.org/10.1116/1.1798811>.
- [52] M. Hou, D.G. Senesky, Operation of ohmic Ti/Al/Pt/Au multilayer contacts to GaN at 600 °C in air, *Appl. Phys. Lett.* 105 (2014), 081905, <https://doi.org/10.1063/1.4894290>.
- [53] N. Goyal, S. Dusari, J. Bardong, F. Medjdoub, A. Kenda, A. Binder, Multilayer Pt/Al based ohmic contacts for AlGaIn/GaN heterostructures stable up to 600 °C ambient air, *Solid-State Electron.* 116 (2016) 107–110, <https://doi.org/10.1016/j.sse.2015.12.002>.
- [54] K. Masahiro, S. Noboru, Effects of temperature, thickness and atmosphere on mixing in Au–Ti bilayer thin films, *J. Mater. Sci.* 28 (1993) 5088–5091, <https://doi.org/10.1007/BF00361184>.
- [55] W.E. Martinez, G. Gregori, T. Mates, Titanium diffusion in gold thin films, *Thin Solid Films* 518 (2010) 2585–2591, <https://doi.org/10.1016/j.tsf.2009.07.187>.
- [56] Y. Hoshino, Y. Saito, J. Nakata, Interdiffusion analysis of Au/Ti and Au/Pt/Ti electrode structures grown on diamond (001) surface by Rutherford backscattering spectroscopy, *Jpn. J. Appl. Phys.* 49 (10) (2010) 101302-1–101302-5, <https://doi.org/10.1143/JJAP.49.101302>.
- [57] J. Sun, R. Sokolovskij, E. Iervolino, Z. Liu, P.M. Sarro, G. Zhang, Suspended AlGaIn/GaN HEMT NO<sub>2</sub> gas sensor integrated with micro-heater, *J. Microelectromech. Syst.* 28 (6) (2019) 997–1004, <https://doi.org/10.1109/JMEMS.2019.2943403>.

**Robert Sokolovskij** received the B.S. degree in electronics engineering from Vilnius University, Vilnius, Lithuania in 2010. Since 2011 he joined Delft University of Technology, Delft, the Netherlands where he obtained the M.S. degree in electrical engineering in 2013 and Ph.D. degree in 2019. From 2014 to 2018 he was also with the State Key Laboratory of Solid-State Lighting, Changzhou, China. From 2018 to 2020 he was also a research assistant at the Southern University of Science and Technology (SUSTech), Shenzhen, China. Since 2020 he is a research assistant professor at the School of Microelectronics, SUSTech. His current research interests include design, fabrication and characterization of wide bandgap gallium nitride (GaN)-based power electronic devices and chemical sensors.

**Hongze Zheng** received the B.S. degree from South University of Science and Technology (SUSTech), Shenzhen, China in July, 2019. Currently he is working as a research assistant at SUSTech. His current research is mainly focused on wide energy gap devices and gas sensors.

**Wenmao Li** received the B.E. degree from Southern University of Science and Technology (SUSTech), Shenzhen, China in July, 2018. He is currently a Ph.D. student in Electronics, Southern University of Science and Technology, Shenzhen, China. His current research interests include wide energy gap devices and sensors.

**Guangnan Zhou** received the B.Sc. degree in physics from University of Science and Technology of China in 2015 and the M.A.Sc degree in materials engineering from the University of British Columbia, Canada, in 2017. He is currently under the joint-PhD program of the University of British Columbia and Southern University of Science and Technology with a focus on p-GaN gate GaN HEMTs for power switching applications. He has an in-depth understanding of GaN device physics, fabrication, characteristics, and reliability, and is co-author of several journal papers.

**Qing Wang** is working as a research associate professor at the School of Microelectronics, Southern University of Science and Technology (SUSTech), China. She received her Ph.D. degree in materials science and engineering from South China University of Technology in 2013. Later she worked at Sino Nitride Semiconductor Co., Ltd for 6 years. Her major research is on GaN power devices and RF devices for power adapter, smart grid, and 5G communication applications.

**Guoqi Zhang** received the Ph.D. degree from the Delft University of Technology, The Netherlands, in 1993. He is a Chair Professor of Micro/Nanoelectronics System Integration and Reliability with the Delft University of Technology. His research interests include multilevel heterogeneous system integration and packaging, wide band gap semiconductors sensors and components, multiphysics and multiscale modeling of micro/nanoelectronics, and digital twin for mission critical multifunctional electronics components and systems. He has authored/coauthored more than 400 scientific publications. He serves as the Deputy Director of the European Center for Micro- and Nano reliability (EUCEMAN), the Co-Chair of the Advisory Board of International Solid-State Lighting Alliance (ISA), and the Secretary General of the International Technology Roadmap of Wide Bandgap Semiconductors (ITRW). He has worked for NXP Semiconductors as the Senior Director of Technology Strategy until 2009 and a Philips Research Fellow until May 2013.

**Hongyu Yu** received his B.Sc., M.Sc., and Ph.D. from Tsinghua University, University of Toronto, and National University of Singapore, respectively. He is currently the professor and dean of the School of Microelectronics, Southern University of Science and Technology, Shenzhen, China. His current research interests include integrated circuit technology and devices, CMOS, new ultra-high-density memory, GaN HEMT devices, and system integration.